Journal of Solid State Electrochemistry
https://doi.org/10.1007/s10008-023-05616-5

ORIGINAL PAPER

Zn-based metal–organic framework with intramolecular hydrogen bond for the electroreduction of CO_2 to formate

Minhong Yan[1] · Ying Yang[1] · Tingting Zhan[1] · Jiayi Luo[1] · Limei Huang[1] · Xiuling Ma[1] · Shengchang Xiang[1]

Received: 31 May 2023 / Revised: 23 July 2023 / Accepted: 25 July 2023

Abstract

Metal–organic frameworks (MOFs) have important research value in the field of electrochemical CO_2 reduction reaction because of their rational design. Here, a new MOF-CH_3 was prepared via a simple solvothermal method by using Zn as the metal center and 1,2,4-triazole and 2-methyl-terephthalic acid as ligands for electrocatalytic CO_2 reduction. The single-crystal X-ray diffraction shows that MOF-CH_3 is N, O-coordinated 3D columnar layer framework with intramolecular hydrogen-bonding interactions. The powder X-ray diffraction for MOF-CH_3 displays the good crystallinity of 24 h in 0.5 mol L^{-1} $KHCO_3$ electrolyte solution. The electrochemical CO_2 reduction reaction tests indicate that the MOF could effectively convert CO_2 to formate, and the highest Faradaic efficiency of formate ($FE_{formate}$) is 76.5% at − 1.37 V (vs. reversible hydrogen electrode) with a partial current density of formate of − 12.1 mA cm^{-2}. The performance of MOF-CH_3 is better than that of the reported other two structural analogues MOF-NH_2 with $FE_{formate}$ of 55.7% at − 1.57 V or MOF-H with $FE_{formate}$ of 73.5% at − 1.37 V in aqueous CO_2-saturated electrolyte solution. The work shows that the performance could be improved by regulating the microenvironment of MOF catalysts.

Keywords Metal − organic frameworks · Electrochemical reduction of CO_2 · Formate · Intramolecular hydrogen bond

Introduction

With the rapid development of the global economy, the consumption of diverse fossil energy sources has been increasing day by day [1–3]. CO_2, as the final product of the burning of fossil fuels, its excessive emission has caused the global warming and other environmental issues [4, 5]. To address the issues, it is an inevitable trend of reducing the emissions of CO_2. Electrochemical CO_2 reduction, which could effectively convert CO_2 to valuable petrochemicals, has been considered as one of the more attractive and promising strategies due to its simple process and mild reaction conditions [6–8]. However, it is still a challenge to achieve a high-efficiency CO_2 reduction with a suitable electrocatalyst which contains high activity and good selectivity, due to the large thermodynamic energy barrier and difficulty of activating stable CO_2 molecules as well as competitive hydrogen evolution reaction [9, 10].

In recent years, various catalysts, such as nanomaterials [11–13], metal [14, 15], transition-metal oxide [16, 17], metal-free materials carbon [18, 19], and metal–organic framework (MOFs) [20, 21], have been explored for electrocatalytic CO_2 conversion [22–24]. Compared with other electrocatalysts, MOFs, as a highly porous material with a periodic network structure formed by the self-assembly of organic ligands and metal ions or clusters, exhibit a hopeful electrocatalyst for CO_2 reduction due to their high surface areas, single active sites, and potential to capture CO_2 [25–27]. However, they often suffer from poor chemical stability in the electrolyte solution and are sensitive to water, severely hindering their industrial use. Recently, balanced hydrogen-bonding interactions between the cationic frameworks and anions have been proposed to enhance the stability of MOFs [28]. And intramolecular hydrogen-bonding interactions (IHBIs) play fundamentally important roles in the fabrication of stable MOFs. To date, improving MOF stability for electrochemical CO_2 reduction through IHBIs has rarely been considered. Because of Zn-based catalysts with high cost-effectiveness and low-activity hydrogen

✉ Limei Huang
lmhuang@fjnu.edu.com

[1] Fujian Key Laboratory of Polymer Materials, College of Chemistry and Materials Science, Fujian Normal University, Fuzhou 350007, China

Published online: 20 September 2023

evolution reaction [29], Zn-MOF-based electrocatalysts of CO_2 reduction have attracted great interest [30–32]. Presently, most reported Zn-MOFs show high selectivity and activity to CO or CH_4 [31, 33, 34], only a few Zn-MOFs [35] exhibit high selectivity of formate which is economically feasible in view of the market value and the energy input. Investigating its reason, the coordination environment of the metal as an active site greatly affects the product selectivity of CO_2 reduction. Therefore, it is significant to design and synthesize new Zn-MOFs with IHBIs for electrocatalytic conversion of CO_2 to formate.

In this work, a new three-dimensional N, O-co-coordinated MOF-CH_3 was obtained using Zn as the metal center and 1,2,4-triazole and 2-methyl terephthalic acid as organic ligands by a simple solvothermal method. The MOF-CH_3 is isostructural with the reported FJU-40-NH_2 (denoted by MOF-NH_2 here) containing IHBIs and FJU-40-H (denoted by MOF-H here) without IHBIs [28]. MOF-CH_3 and MOF-NH_2 show far better chemical stability than MOF-H in an electrolyte solution. The electrochemical CO_2 reduction test displays that all the N,O-co-coordinated Zn-based MOFs exhibit specific selectivity for conversion CO_2 to formate with the faradaic efficiency (FE) more than 55% at the optimal potential, which is consistent with the reported N,O-coordinated Zn-based MOFs [35], but different from the reported N- or O-coordinated Zn-based MOFs catalysts with the primary product of CO or CH_4 [31, 33, 34]. The above results indicate that the microenvironment of the catalyst could affect the electroreduction of CO_2. The $FE_{formate}$ of 76.5% for MOF-CH_3 is lower than that for MOF materials such as Zn-MOF [35], Bi-BTC-D-3.75 [36], and MIL-68(In)-NH_2 [37], but higher than that for $(Me_2NH_2^+)$[InIII-(TTFTB)]·0.7C_2H_5OH·DMF [38], Cu-MOF/GO [39], and MFM-300(In)-t/CP [40]. Although there are relatively poor CO_2 reaction activities for MOF-CH_3 in comparison with the reported advanced catalysts, this work provided a novel Zn-based MOF catalyst with IHBIs for electrochemical conversion of CO_2 to formate.

Experiment

Materials

All reagents and chemicals were obtained commercially and used without further purification. 1,2,4-triazole, terephthalic acid, 2-amino-terephthalic acid, 2-methyl-terephthalic acid, zinc nitrate hexahydrate, and *N*, *N*-dimethylformamide (DMF) were purchased from Sinopharm Chemical Reagent Co., Ltd. Nafion 117 proton exchange membrane and NafionD-521 dispersion (5 wt% in lower aliphatic alcohols and water) were purchased from Shanghai Hesen Electric Co., Ltd.

Instrumentation

Powder X-ray diffraction (PXRD) was carried out with a PANalytical X'Pert^3 diffractometer equipped with a Cu-sealed tube ($\lambda = 1.541874$ Å) at 40 kV and 40 mA over the 2θ range of 5–30°. The simulated PXRD pattern was produced by using the Mercury V1.4 program and single-crystal diffraction data. Thermal analysis was carried out on a METTLER TGA/SDTA 851 thermal analyzer from 30 to 600 °C at a heating rate of 10 °C min^{-1} under N_2 flow. Fourier transform infrared spectra (FT-IR, KBr pellet) were measured in the range of 400–4000 cm^{-1} by a Nicolet 5700 FT-IR. Elemental (C, H, N) analytical data were obtained on a Perkin-Elmer model 240C elemental analyzer. Electrochemical test data were recorded with a Versa STAT 3F electrochemical workstation (Princeton Instruments, USA). All the gas products (CO and H_2) were quantified with a gas chromatography (PANNA-A60), which was equipped with a thermal conductivity detector and flame ionization detector, and N_2 was used as carrier gas. Liquid products were analyzed by quantitative ^{1}H-nuclear magnetic resonance (NMR, Bruker AVNANCE-400) using deuterium oxide as an internal standard.

Synthesis of MOF-R (R = CH_3, H_2, H) for the electroreduction of CO_2

MOF-R (R = CH_3, H_2, H) were prepared via solvothermal reaction. The detailed information was shown in Supplementary Information, including synthesis, SCXRD analysis, electrochemical measurements, and product analysis.

Results and discussion

Structures and characterization of MOF-R (R = CH_3, NH_2, H)

As illustrated in Fig. 1a, a series of Zn-based MOFs (MOF-R, R = CH_3, NH_2, H) were prepared by a facile one-step solvothermal procedure with zinc nitrate and organic ligands. The images of scanning electron microscopy (SEM) show that all the MOFs are relatively regular block structures (Fig. S1), wherein MOF-CH_3 is a new MOF material. SCXRD patterns of the obtained MOF-CH_3 could be ascribed to a structural type with a tetragonal P4/nnc space group which is consistent with MOF-NH_2 (Table S1). Each Zn^{II} atom with tetrahedron geometry (Table S2 and S3) is coordinated with three N atoms from three 1,2,4-triazole ligands molecules and two O atoms from a 2-methyl-terephthalic acid ligand (Fig. 1a). And

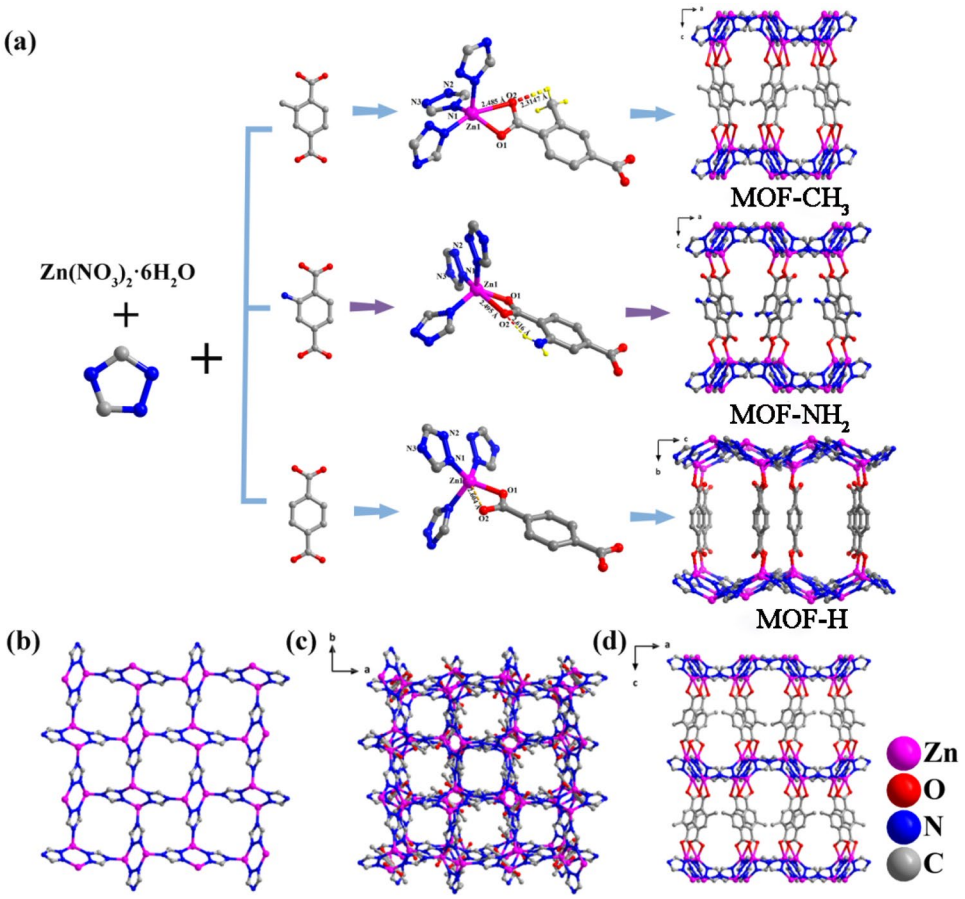

Fig. 1 **a** Synthesis and structure illustration of MOF-R (R = CH_3, NH_2, H), **b** [Zn_2(1,2,4-triazole)$_2$] units connect to each other to form a two-dimensional layer of MOF-CH_3, and **c**, **d** three-dimensional open framework pillared by 2-methyl-terephthalic acid of MOF-CH_3

the two Zn^{II} atoms are joined by two 1,2,4-triazole ligands to form a [Zn_2(1,2,4-triazole)$_2$] unit (Fig. 1b), which connect to each other to extend further into a waved two-dimensional layer. These layers are further supported by 2-methyl-terephthalic acid ligands via Zn–O coordinated bonds to form a three-dimensional columnar layer framework (Fig. 1c, d). These Zn-MOFs have almost the same physical structure as MOF-NH_2 and MOF-H, which are all columnar structures constructed with [Zn_2(1,2,4-triazole)$_2$]$_n$ as layers and 2-methyl-terephthalic acid as column (Fig. 1a). Nevertheless, their structures are slightly different due to the differences in the functional groups of terephthalic acid-R linker (Fig. 1a). For MOF-CH_3 or MOF-NH_2, the IHBIs with d[O(−COO)···H(−CH_3)] = 2.3147 Å or d[O(-COO)···H(-NH_2)] = 2.616 Å are formed between hydrogen atoms of −CH_3 or NH_2 and carboxyl oxygen atoms (Fig. 1a), which could shorten the distance of Zn1-O2. Specifically, the Zn1-O2 bond lengths in MOF-CH_3, MOF-NH_2, and MOF-H are 2.485 Å, 2.495 Å, and 2.604 Å, respectively (Table S2). A shorter Zn1-O2 bond length could make MOF-CH_3 and MOF-NH_2 more stable than MOF-H [28], which was confirmed by the subsequent stability test in $KHCO_3$ electrolyte solutions via powder X-ray diffraction (PXRD).

The PXRD data for the as-prepared MOF-CH_3 or MOF-NH_2 materials (Fig. 2a, b) has typical diffraction peaks at the 2θ of 6.387°, 9.128°, 13.120°, and 15.17°, which match well with the simulated PXRD pattern of the main crystal faces (002), (102), (200), and (211), respectively. MOF-H also shows the crystal faces (020), (011), (101), and (111) at the typical diffraction peaks of 2θ = 6.611°, 9.735°, 12.763°, and 13.117°, respectively (Fig. 2c). These results indicate the successful synthesis of MOF-R. The thermal stability of MOF-R was measured by thermogravimetric (TG) analysis. TG curve results display that MOF-R has pretty similar weightlessness tracks up before 600 °C (Fig. 2d). For MOF-CH_3, the first weight loss at 123 °C is the loss of DMF molecules. Then, the plateau was maintained until the framework began to decompose at around 369 °C. The MOF-NH_2 and MOF-H lose the first weightlessness before 100 °C, which could be ascribed to the loss of water molecules in the pore channel. For MOF-NH_2, the second weight loss at 123 ℃ is the loss of DMF molecules. The last weight loss over 322 ℃ corresponds to the decomposition of the framework. For MOF-H, the molecules of DMF evaporate at ~ 112 ℃, and when heated above 345 ℃, the organic ligands start the decomposition, and the framework collapse. These results suggest that the MOFs possess excellent

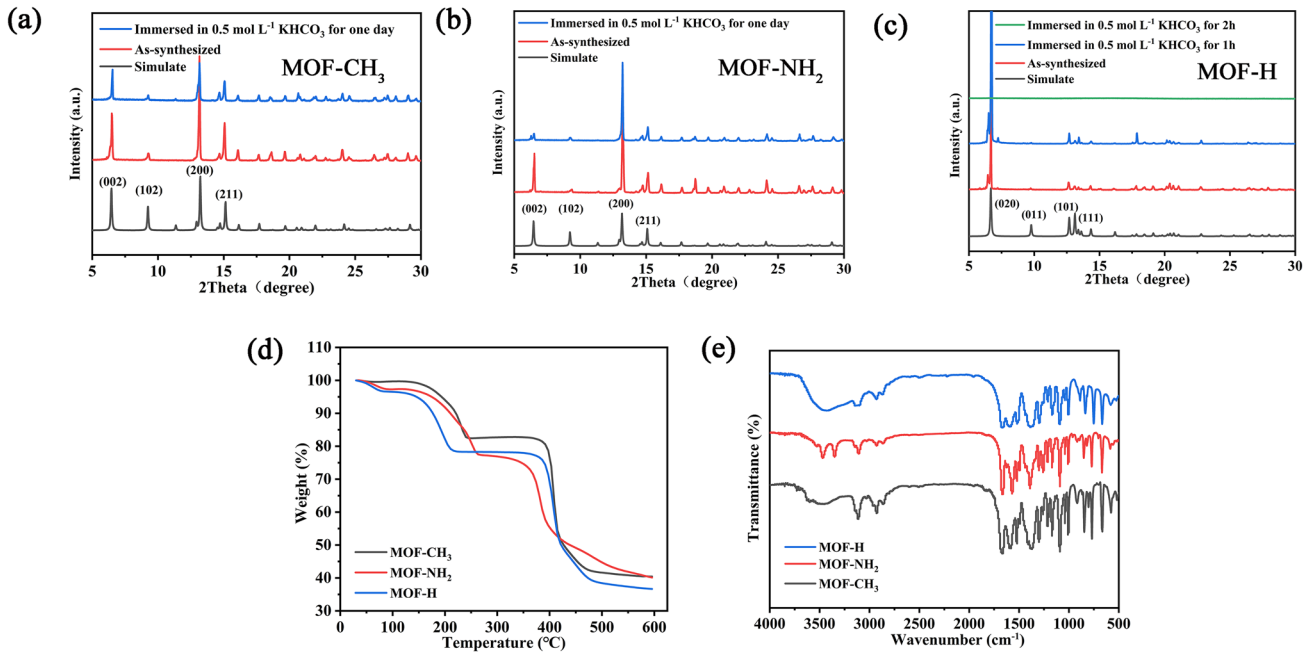

Fig. 2 **a**–**c** Powder X-ray diffraction patterns, **d** thermogravimetric curves, and **e** Fourier transform infrared spectroscopy spectra of MOF-R (R = CH_3, NH_2, H)

thermal stability. The characteristic temperatures and final weight losses of all samples are also stated in Table S4. The Fourier transform infrared spectroscopy (FT-IR) spectrums of MOF-R are displayed in Fig. 2e. All the MOFs show C-N peak at about 1130 cm^{-1} for 1,2,4-triazole ligand and the characteristic peaks of C = O/C-O, respectively, at about 1720/1100 cm^{-1} for terephthalic acid ligand. For MOF-CH_3, the characteristic peaks of $-CH_3$ group are at 2940 cm^{-1}, 2860 cm^{-1}, and 1380 cm^{-1}. There are two peaks at 3470 cm^{-1} and 3340 cm^{-1}1 with moderate intensity, which correspond to N–H antisymmetric stretching vibration and symmetric stretching vibration on $-NH_2$ functional group of MOF-NH_2, respectively. In addition, we found that MOF-CH_3 and MOF-NH_2 have blunt peaks of O–H stretching vibration intramolecular hydrogen bonds at 3610 cm^{-1} and 3530 cm^{-1}[28], while MOF-H does not, which is consistent with the crystal structure analysis described in Fig. 1a.

Electrochemical measurements and CO_2RR performance

The stability of the three MOFs immersed in 0.5 mol mL^{-1} $KHCO_3$ electrolyte solution was analyzed, as shown in Fig. 2a–c. The results show that MOF-CH_3 and MOF-NH_2 in the electrolyte solution could maintain good crystallinity for 24 h, while there are basically no diffraction peaks for MOF-H after soaking for 2 h. The stability differences of the MOFs in the electrolyte solutions should be closely related to the presence of IHBIs in their structures. For MOF-CH_3 or MOF-NH_2, the distance between Zn1-O2 is shortened due to the presence of IHBIs. A shorter Zn1-O2 distance could protect Zn atoms from water attack, resulting in better stability of MOF-CH_3 or MOF-NH_2 than MOF-H in electrolyte solutions.

Electrochemical CO_2 reduction tests were conducted in 0.5 mol mL^{-1} $KHCO_3$ electrolyte solution (pH = 7.2) via a liquid H-type electrochemical cell with successive CO_2 bubbling at a flow rate of 20 mL min^{-1} [41]. The gaseous and liquid reduction products were respectively detected and quantified by gas chromatography and ^{1}H-nuclear magnetic resonance (^{1}H-NMR), and details were provided in supporting information. The cyclic voltammograms curves for MOF-CH_3 and MOF-H (Fig. 3a, b) with the redox current peaks of Zn(II) reduced to Zn(I) [31, 35, 42] show that the onset potentials of MOF-R under CO_2 atmosphere are more positive than that in Ar condition, which indicates their activities are originated from the CO_2 conversion [43, 44]. Although MOF-NH_2 has similar CV curves in Ar and CO_2 condition, the current density values in the CO_2 condition is higher than that in the Ar condition when the potential values surpass 1 V (Fig. 3c), indicating CO_2 reduction reaction still is the superior reaction. Moreover, MOF-CH_3 exhibits slightly larger current densities at high potential than MOF-NH_2 or MOF-H from linear sweep voltammetry curves (Fig. S2). In order to study CO_2 reduction activity and selectivity, chronoamperometry tests were conducted at different potentials (Fig. S3). Formate, CO, and H_2 are the products of CO_2 reduction over the MOF-R materials at each

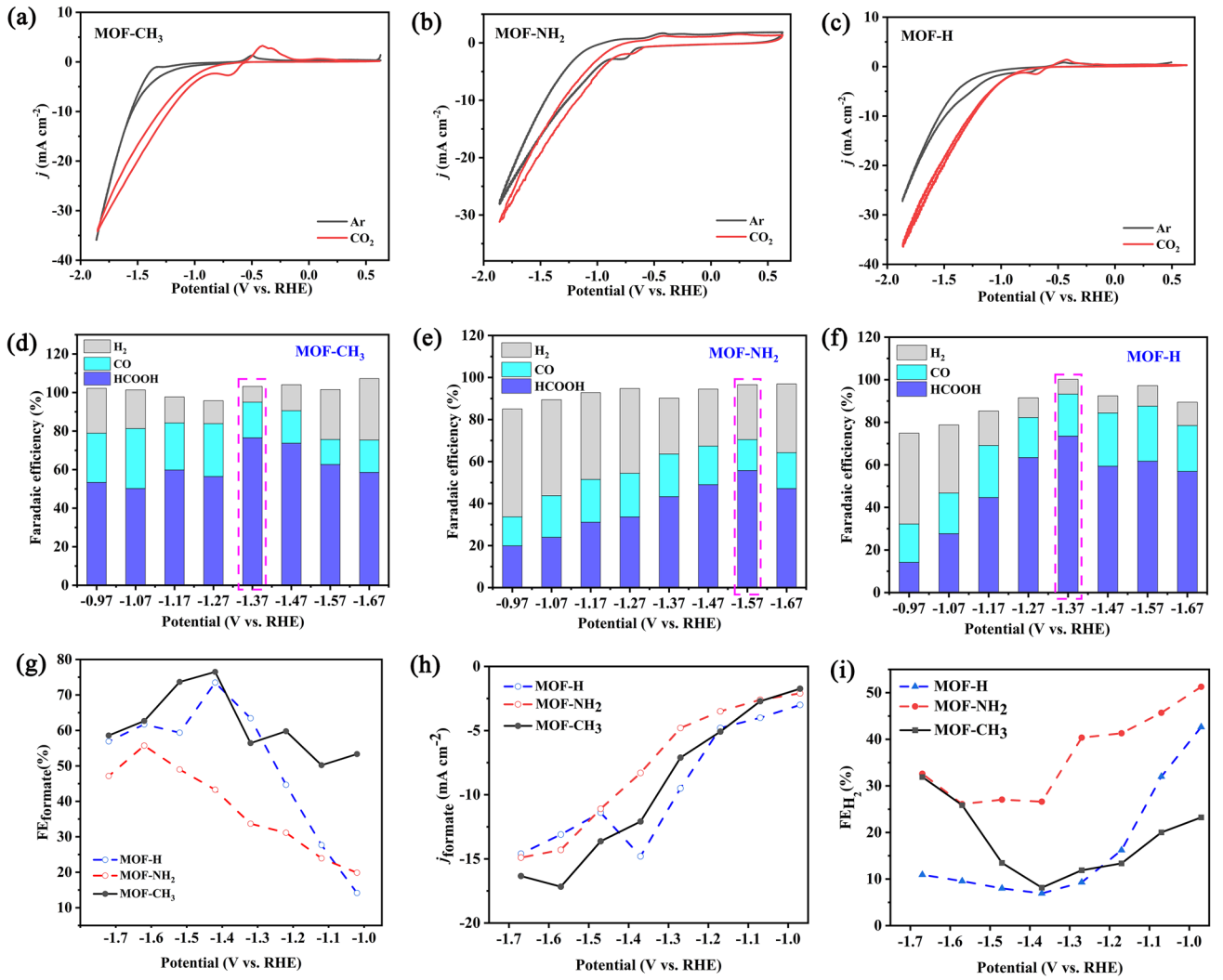

Fig. 3 **a–c** Cyclic voltammograms curves in Ar-(black line) or CO_2-(red line) saturated 0.5 mol L^{-1} $KHCO_3$ solutions with a scan rate of 50 mV s^{-1}, **d–f** faradaic efficiency of different products, **g** faradaic efficiency of formate, **h** partial current densities of formate, and **i** faradaic efficiency of H_2 for MOF-R (R = CH_3, NH_2, H) at given potentials

potential from − 0.97 to − 1.67 V vs. RHE (reversible hydrogen electrode, the same below) (Fig. 3d–f), and formate is the primary product at the most given potential, especially MOF-CH_3 (Fig. 3d). The detailed data in Fig. 3d–f has also been shown in Table S5. In addition, the gas chromatograms of the gaseous products formed at the optimum potential were provided in Fig. S4 for explicitness, and ^{1}H-NMR of the liquid phase products was shown in Fig. S5a. To confirm the formate from the electroreduction of CO_2, isotopic labeling tests were further performed by using the mixture of $^{13}CO_2/^{12}CO_2$ as the feedstock. The ^{1}H-NMR signals of H^{13}COOH (Fig. S5b) illustrate that the formate originated from the CO_2 reduction.

As shown in Fig. 3g, h, the highest $FE_{formate}$ for MOF-CH_3 and MOF-H is, respectively, 76.5% and 73.5% at − 1.37 V, with the partial current density of formate ($j_{formate}$) of − 12.1 mA cm^{-2} and $^-$14.0 mA cm^{-2}, respectively. The maximum $FE_{formate}$ for MOF-NH_2 is 55.7% at − 1.57 V with $j_{formate}$ of − 14.5 mA cm^{-2}. As shown in Fig. 3g, the MOF-CH_3 shows good selectivity of formate with $FE_{formate}$ of more than 50% at all applied potentials, while poorer formate selectivity of MOF-NH_2 was obtained than that of MOF-CH_3 or MOF-H. Also, the FE_{H2} for MOF-NH_2 is up to 40–50% in the low potential range of − 0.97 to − 1.27 V, and MOF-H shows high FE_{H2} at − 0.97 V (Fig. 3i). The formate concentration of MOF-CH_3 is higher than MOF-NH_2 or MOF-H in a wide potential ranging from − 0.97 to − 1.67 V except − 1.27 V (Fig. S6). The concentration of formate for MOF-CH_3 is 11.1 mmol L^{-1} at − 1.37 V, while that for MOF-NH_2 and MOF-H is 7.0 mmol L^{-1} and 9.6 mmol L^{-1}, respectively. Taken overall, MOF-CH_3 is more efficient electrocatalysts for CO_2 reduction than MOF-NH_2 or MOF-H.

A comparison of Zn-based MOFs and complex electrocatalysts for CO_2 reduction was summarized in Table S6. These N,O-co-coordinated Zn-based MOFs exhibit specific selectivity for formate at the optimum potential ($FE > 55\%$), different from the reported N- or O-coordinated Zn-based MOF catalysts with the primary product of CO or CH_4 [31, 33, 34]. Although there is a relatively poor CO_2 reduction selectivity for MOF-CH_3 in comparison with the reported N, O-coordinated Zn-based MOFs [35], this work provided a novel example of Zn-MOF catalysts with IHBIs for electrochemical conversion of CO_2 to formate.

To further probe the catalytic activity of Zn-MOFs during CO_2 reduction, the Tafel plots, electrochemical impedance spectroscopy (EIS), the electrochemical active surface area (ECSA), and turnover frequency (TOF) [45] were studied. The reaction kinetics of the CO_2 reduction process was explored by the Tafel analysis. The low Tafel slope means fast dynamics and better electrocatalytic performance. As illustrated in Fig. 4a, MOF-CH_3 displayed a Tafel slope of 232.7 mV dec^{-1}, slightly smaller than MOF-NH_2 (346.9 mV dec^{-1}) and MOF-H (234.7 mV dec^{-1}). This indicates that MOF-CH_3 has a relatively faster kinetics and excellent electrocatalytic performance for CO_2 reduction. In addition, the electron transfer behavior of MOF-R during CO_2 reduction was studied via EIS measurement, which is displayed in Fig. 4b. MOF-CH_3 has a lower semicircular radius (R) of ~ 700 Ω than MOF-NH_2 or MOF-H at − 0.37 V. The smaller R reflects the much favorable charge transfer kinetics, which also reveals that MOF-CH_3 has better electrochemical capabilities [46, 47]. Additionally, the electrochemical double-layer capacitance (C_{dl}) measured by CV at different scan rates (Fig. S7) was used to evaluate the ECSA of the Zn-MOF electrocatalysts. A higher C_{dl} generally means a higher ECSA which illustrates more exposed active sites [48]. The result showed that C_{dl} value for MOF-CH_3, MOF-NH_2, and MOF-H is 4.0, 6.5, and 6.25 mF cm^{-2}, respectively (Fig. 4c). Although MOF-NH_2 or MOF-H has an obviously higher ECSA than MOF-CH_3, the two electrocatalysts do not exhibit better conversion performance of CO_2 to formate, as could be explained by more reaction active sites given to HER or the conversion of CO_2 to CO at most applied potentials, based on the FE values of the products. Besides, TOF was used to evaluate the intrinsic activity of electrocatalysts. These TOF results for MOF-CH_3 are better than that for MOF-NH_2 or MOF-H at most given potentials (Fig. 4d), which could verify that MOF-CH_3 has higher intrinsic actives.

Although the metal center for these MOFs is the same and their structure is similar, these MOFs show different effects of CO_2 reduction. Apart from the presence or absence of intramolecular hydrogen bonds which mainly affect the stability, they also possess different functional groups (−CH_3, −NH_2, −H) with regard to microenvironment. Thus, we further explore the effect of functional groups. And contact angle tests were performed to analyze the hydrophilicity of the Zn-MOFs. As shown in Fig. S8, the contact

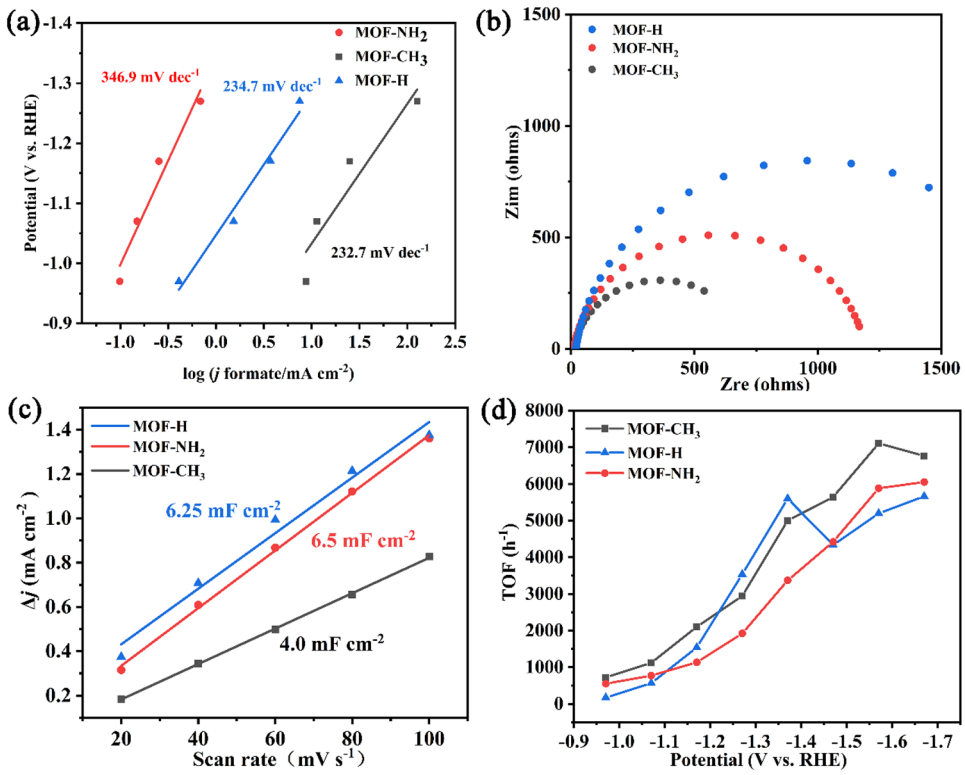

Fig. 4 **a** Tafel plots, **b** electrochemical impedance spectroscopy spectra at − 0.37 V, **c** charging current density at different scan rates, and **d** turnover frequency plots for the generation of formate for MOF-R (R = CH_3, NH_2, H)

angle of 44.2° for MOF-CH_3 is larger than that of the other two MOFs, indicating that the hydrophilicity of MOF-CH_3 is poorer than the others. The introduction of hydrophobic groups ($-CH_3$) could make MOFs show good chemical stability and avoid the attack from water to generate H_2 to some extent, which is helpful for CO_2 reduction [49]. FE_{H2} of MOF-CH_3, that is lower than that of MOF-NH_2 at most given different potentials (Fig. 3i), also illustrated that MOF-CH_3 could effectively inhibit the hydrogen evolution reaction. To sum up, favorable charge transfer kinetics and intrinsic activity as well as hydrophobicity let MOF-CH_3 improve electrocatalytic CO_2 reduction in comparison with the other two structural analogues. It is clear that the performance could be improved by regulating the coordination microenvironment of MOF catalysts.

Conclusions

In summary, a series of N, O-coordinated Zn-based isostructuralism MOF catalysts were obtained by a simple solvothermal method for selective electroconversion of CO_2 to formate under ambient conditions. Among them, MOF-CH_3 is a new MOF with IHBI distance of 2.3147 Å from the SCXRD analyses. MOF-NH_2 also exists as an intramolecular hydrogen bond with the distance of 2.616 Å, while MOF-H does not. PXRD results indicate that the presence of IHBIs in MOFs is helpful for keeping the good crystallinity in electrolyte solution. The related electrochemical tests for CO_2 reduction show that the catalytic performance of MOF-CH_3 with $FE_{formate}$ 76.5% at − 1.37 V is better than that of MOF-NH_2 with $FE_{formate}$ of 55.7% at − 1.57 V or MOF-H with $FE_{formate}$ of 73.5% at − 1.37 V. According to the analyses of EIS, TOF, and contact angle, it was found that MOF-CH_3 possesses the lowest *R* of ~ 700 Ω, high intrinsic actives, and the largest contact angle of 44.2°. The introduction of IHBIs and hydrophobic groups ($-CH_3$) may be helpful for CO_2 reduction. This work provides a novel Zn-MOF catalyst for the electroreduction of CO_2 to formate.

Supplementary Information The online version contains supplementary material available at https://doi.org/10.1007/s10008-023-05616-5.

Funding The authors gratefully acknowledge the financial support from the National Natural Science Foundation of China (No. 21975044, 21971038, and 21922810) and the Natural Science Foundation of Fujian Province (2020J01151).

References

1. Xiao J, Chevallier F, Gomez C, Guanter L, Hicke JA, Huete AR, Ichii K, Ni W, Pang Y, Rahman AF, Sun G, Yuan W, Zhang L, Zhang X (2019) Remote sensing of the terrestrial carbon cycle: a review of advances over 50 years. Remote Sens Environ 233:111383
2. Li Y, Wei B, Zhu M, Chen J, Jiang Q, Yang B, Hou Y, Lei L, Li Z, Zhang R, Lu Y (2021) Synergistic effect of atomically dispersed Ni-Zn pair sites for enhanced CO_2 electroreduction. Adv Mater 33:2102212
3. Hu XM, Ronne MH, Pedersen SU, Skrydstrup T, Daasbjerg K (2017) Enhanced catalytic activity of cobalt porphyrin in CO_2 electroreduction upon immobilization on carbon materials. Angew Chem Int Ed 56:6468–6472
4. Li X, Wang S, Li L, Sun Y, Xie Y (2020) Progress and perspective for in situ studies of CO_2 reduction. J Am Chem Soc 142:9567–9581
5. Xu Y, Zhou Z, Zou M, Liu Y, Zheng Y, Yang Y, Lan S, Lan J, Nan C-W, Lin Y-H (2022) Multi-field driven hybrid catalysts for CO_2 reduction: progress, mechanism and perspective. Mater Today 54:225–246
6. Yaashikaa PR, Senthil Kumar P, Varjani SJ, Saravanan A (2019) A review on photochemical, biochemical and electrochemical transformation of CO_2 into value-added products. J CO_2 Util 33:131–147
7. Lee M-Y, Park KT, Lee W, Lim H, Kwon Y, Kang S (2019) Current achievements and the future direction of electrochemical CO_2 reduction: a short review. Crit Rev Environ Sci Technol 50:769–815
8. Wang YR, Huang Q, He CT, Chen Y, Liu J, Shen FC, Lan YQ (2018) Oriented electron transmission in polyoxometalate-metalloporphyrin organic framework for highly selective electroreduction of CO_2. Nat Commun 9:4466
9. Zhao Y, Zheng L, Jiang D, Xia W, Xu X, Yamauchi Y, Ge J, Tang J (2021) Nanoengineering metal-organic framework-based materials for use in electrochemical CO_2 reduction reactions. Small 17:2006590
10. Baddour FG, Roberts EJ, To AT, Wang L, Habas SE, Ruddy DA, Bedford NM, Wright J, Nash CP, Schaidle JA, Brutchey RL, Malmstadt N (2020) An exceptionally mild and scalable solution-phase synthesis of molybdenum carbide nanoparticles for thermocatalytic CO_2 hydrogenation. J Am Chem Soc 142:1010–1019
11. Zhang W, Yang S, Jiang M, Hu Y, Hu C, Zhang X, Jin Z (2021) Nanocapillarity and nanoconfinement effects of pipet-like bismuth@carbon nanotubes for highly efficient electrocatalytic CO_2 reduction. Nano Lett 21:2650–2657
12. Zhang W, Xia Y, Chen S, Hu Y, Yang S, Tie Z, Jin Z (2022) Single-atom metal anchored Zr(6)-cluster-porphyrin framework hollow nanocapsules with ultrahigh active-center density for electrocatalytic CO_2 reduction. Nano Lett 22:3340–3348
13. Yang S, Jiang M, Wang M, Wang L, Song X, Wang Y, Tie Z, Jin Z (2023) Rational design and synergistic effect of ultrafine Ag nanodots decorated fish-scale-like Zn nanoleaves for highly selective electrochemical CO_2 reduction. Nano Res 16(7):8910–8918
14. Torbensen K, Joulié D, Ren S, Wang M, Salvatore D, Berlinguette CP, Robert M (2020) Molecular catalysts boost the rate of electrolytic CO_2 reduction. ACS Energy Lett 5:1512–1518
15. Liu M, Pang Y, Zhang B, De Luna P, Voznyy O, Xu J, Zheng X, Dinh CT, Fan F, Cao C, de Arquer FP, Safaei TS, Mepham A, Klinkova A, Kumacheva E, Filleter T, Sinton D, Kelley SO, Sargent EH (2016) Enhanced electrocatalytic CO_2 reduction via field-induced reagent concentration. Nature 537:382–386
16. Atrak N, Tayyebi E, Skúlason E (2021) Effect of co-adsorbed water on electrochemical CO_2 reduction reaction on transition metal oxide catalysts. Appl Surf Sci 570:151031
17. Ait Ahsaine H, BaQais A (2023) Metal and metal oxide electrocatalysts for the electrochemical reduction of CO_2-to-C1 chemicals: are we there yet? Green Chem Lett Rev 16:2160215

18. Zhang L, Lin CY, Zhang D, Gong L, Zhu Y, Zhao Z, Xu Q, Li H, Xia Z (2019) Guiding principles for designing highly efficient metal-free carbon catalysts. Adv Mater 31:1805252
19. Sun X, Kang X, Zhu Q, Ma J, Yang G, Liu Z, Han B (2016) Very highly efficient reduction of CO_2 to CH_4 using metal-free N-doped carbon electrodes. Chem Sci 7:2883–2887
20. Xiang H, Shao Y, Ameen A, Chen H, Yang W, Gorgojo P, Siperstein FR, Fan X, Pan Q (2020) Adsorptive separation of C_2H_6/C_2H_4 on metal-organic frameworks (MOFs) with pillared-layer structures. Sep Purif Technol 242:116819
21. Wang H, Wu X, Liu G, Wu S, Xu R (2022) Bimetallic MOF derived nickel nanoclusters supported by nitrogen-doped carbon for efficient electrocatalytic CO_2 reduction. Nano Res 16:4546–4553
22. Yan T, Wang P, Xu ZH, Sun WY (2022) Copper (II) frameworks with varied active Site distribution for modulating selectivity of carbon dioxide electroreduction. ACS Appl Mater Interfaces 14:13645–13652
23. Dou S, Song J, Xi S, Du Y, Wang J, Huang ZF, Xu ZJ, Wang X (2019) Boosting electrochemical CO_2 reduction on metal-organic frameworks via ligand doping. Angew Chem Int Ed 58:4041–4045
24. Masoomi MY, Morsali A, Dhakshinamoorthy A, Garcia H (2019) Mixed-metal MOFs: unique opportunities in metal-organic framework (MOF) functionality and design. Angew Chem Int Ed 58:15188–15205
25. Cao L, Wu X, Liu Y, Mao F, Shi Y, Li J, Zhu M, Dai S, Chen A, Liu PF, Yang HG (2022) Electrochemical conversion of CO_2 to syngas with a stable H_2/CO ratio in a wide potential range over ligand-engineered metal–organic frameworks. J Mater Chem A 10:9954–9959
26. Wu Q, Xie R-K, Mao M-J, Chai G-L, Yi J-D, Zhao S-S, Huang Y-B, Cao R (2020) Integration of strong electron transporter tetrathiafulvalene into metalloporphyrin-based covalent organic framework for highly efficient electroreduction of CO_2. ACS Energy Lett 5:1005–1012
27. Zhai S, Sun J, Sun L, Yang L, Tu R, Jiang S, Yu T, Wu H, Liu C, Li Z, Zhai D, Li Y, Ren G, Deng W (2023) Heteronuclear dual single-atom catalysts for ambient conversion of CO_2 from air to formate. ACS Catal 13:3915–3924
28. Yao Z, Chen Y, Liu L, Wu X, Xiong S, Zhang Z, Xiang S (2016) Direct evidence of CO_2 capture under low partial pressure on a pillared metal-organic framework with improved stabilization through intramolecular hydrogen bonding. ChemPlusChem 81:850–856
29. Qin B, Li Y, Fu H, Wang H, Chen S, Liu Z, Peng F (2018) Electrochemical reduction of CO_2 into tunable syngas production by regulating the crystal facets of earth-abundant Zn catalyst. ACS Appl Mater Interfaces 10:20530–20539
30. Choi I, Jung YE, Yoo SJ, Kim JY, Kim H-J, Lee CY, Jang JH (2017) Facile synthesis of M-MOF-74 (M=Co, Ni, Zn) and its application as an electrocatalyst for electrochemical CO_2 conversion and H_2 production. J Electrochem Sci Technol 8:61–68
31. Wang Y, Hou P, Wang Z, Kang P (2017) Zinc imidazolate metal-organic frameworks (ZIF-8) for electrochemical reduction of CO_2 to CO. ChemPhysChem 18:3142–3147
32. Inge AK, Koppen M, Su J, Feyand M, Xu H, Zou X, O'Keeffe M, Stock N (2016) Unprecedented topological complexity in a metal-organic framework constructed from simple building units. J Am Chem Soc 138:1970–1976
33. Jiang X, Li H, Xiao J, Gao D, Si R, Yang F, Li Y, Wang G, Bao X (2018) Carbon dioxide electroreduction over imidazolate ligands coordinated with Zn(II) center in ZIFs. Nano Energy 52:345–350
34. Kang X, Zhu Q, Sun X, Hu J, Zhang J, Liu Z, Han B (2016) Highly efficient electrochemical reduction of CO_2 to CH_4 in an ionic liquid using a metal-organic framework cathode. Chem Sci 7:266–273
35. Yang Y, Huang J, Zou Y, Li Y, Zhan T, Huang L, Ma X, Zhang Z, Xiang S (2023) N, O-coordinated Zn-MOFs for selective conversion of CO_2 to formate. Appl Surf Sci 618:156664
36. Zhang X, Zhang Y, Li Q, Zhou X, Li Q, Yi J, Liu Y, Zhang J (2020) Highly efficient and durable aqueous electrocatalytic reduction of CO_2 to HCOOH with a novel bismuth–MOF: experimental and DFT studies. J Mater Chem A 8:9776–9787
37. Wang Z, Zhou Y, Xia C, Guo W, You B, Xia BY (2021) Efficient electroconversion of carbon dioxide to formate by a reconstructed amino-functionalized indium-organic framework electrocatalyst. Angew Chem Int Ed 60:19107–19112
38. Zhou Y, Liu S, Gu Y, Wen GH, Ma J, Zuo JL, Ding M (2021) In(III) metal-organic framework incorporated with enzyme-mimicking nickel bis(dithiolene) ligand for highly selective CO_2 electroreduction. J Am Chem Soc 143:14071–14076
39. Hwang SM, Choi SY, Youn MH, Lee W, Park KT, Gothandapani K, Grace AN, Jeong SK (2020) Investigation on electroreduction of CO_2 to formic acid using Cu_3Btc_2 metal-organic framework (Cu-MOF) and graphene oxide. ACS Omega 5:23919–23930
40. Kang X, Wang B, Hu K, Lyu K, Han X, Spencer BF, Frogley MD, Tuna F, McInnes EJL, Dryfe RAW, Han B, Yang S, Schroder M (2020) Quantitative electro-reduction of CO_2 to liquid fuel over electro-synthesized metal-organic frameworks. J Am Chem Soc 142:17384–17392
41. Jia M, Hong S, Wu TS, Li X, Soo YL, Sun Z (2019) Single Sb sites for efficient electrochemical CO_2 reduction. Chem Commun 55:12024–12027
42. Wu XQ, Liu Y, Feng PQ, Wei XH, Yang GM, Qiu XH, Ma JG (2019) Design of a Zn-MOF biosensor via a ligand "lock" for the recognition and distinction of s-containing amino acids. Chem Commun 55:4059–4062
43. Zhang Y, Dong LZ, Li S, Huang X, Chang JN, Wang JH, Zhou J, Li SL, Lan YQ (2021) Coordination environment dependent selectivity of single-site-Cu enriched crystalline porous catalysts in CO_2 reduction to CH_4. Nat Commun 12:6390
44. Zou Y, Zhan T, Yang Y, Fan Z, Li Y, Zhang Y, Ma X, Chen Q, Xiang S, Zhang Z (2022) Single-phase proton- and electron-conducting Ag-organic coordination polymers for efficient CO_2 electroreduction. J Mater Chem A 10:3216–3225
45. Tao H, Fan Q, Ma T, Liu S, Gysling H, Texter J, Guo F, Sun Z (2020) Two-dimensional materials for energy conversion and storage. Prog Mater Sci 111:100637
46. Cao C, Ma DD, Gu JF, Xie X, Zeng G, Li X, Han SG, Zhu QL, Wu XT, Xu Q (2020) Metal-organic layers leading to atomically thin bismuthene for efficient carbon dioxide electroreduction to liquid fuel. Angew Chem Int Ed 59:15014–15020
47. Zhang M, Lin Q, Wu W, Ye Y, Yao Z, Ma X, Xiang S, Zhang Z (2020) Isostructural MOFs with higher proton conductivity for improved oxygen evolution reaction performance. ACS Appl Mater Interfaces 12:16367–16375
48. Li F, Gu GH, Choi C, Kolla P, Hong S, Wu T-S, Soo Y-L, Masa J, Mukerjee S, Jung Y, Qiu J, Sun Z (2020) Highly stable two-dimensional bismuth metal-organic frameworks for efficient electrochemical reduction of CO_2. Appl Catal B 277:119241
49. Li XX, Liu J, Zhang L, Dong LZ, Xin ZF, Li SL, Huang-Fu XQ, Huang K, Lan YQ (2019) Hydrophobic polyoxometalate-based metal-organic framework for efficient CO_2 photoconversion. ACS Appl Mater Interfaces 11:25790–25795